Eur. Phys. J. AP **20**, 9–14 (2002)
DOI: 10.1051/epjap:2002070

THE EUROPEAN PHYSICAL JOURNAL
APPLIED PHYSICS

Enhancement of longitudinal Kerr rotation in Fe/Al_2O_3 composite multilayers

A. Bourzami[1,a], O. Lenoble[2], J.F. Bobo[3], A. Layadi[1], and M. Piecuch[2]

[1] Institut de Physique, Université Ferhat Abbas de Sétif, 19000, Algeria
[2] LPM-UMR CNRS 7556, Université Henri Poincaré de Nancy 1, BP 239, 54506 Vandœuvre-lès-Nancy Cedex, France
[3] LPMC-UMR CNRS 5830-INSA, Dépt. Génie Physique, 31077 Toulouse Cedex 4, France

Received: 4 January 2002 / Received in final form: 29 July 2002 / Accepted: 31 July 2002
Published online: 1 October 2002 –

Abstract. We present experimental results on longitudinal magneto-optic Kerr effect in composite systems based on thin Fe layers associated with amorphous alumina (Al_2O_3). $[Al_2O_3/Fe]_m$-samples ($m = 1, 2$) have been prepared by rf magnetron sputtering onto Si(100) substrate. We have investigated the effect of the Al_2O_3 and Fe thicknesses on the Kerr rotation. The geometry of the multilayers is predicted theoretically by using deduced experimental magneto-optical constants. It will be shown how large Kerr rotation values can be obtained by adjusting sample parameters. For instance, a Kerr rotation close to 7° has been observed from an $Al_2O_3/Fe/Al_2O_3/Fe/Si$ multilayer. The reflectivity and the figure of merit are discussed as a function of the Al_2O_3 thickness.

PACS. 78.20.Ls Magnetooptical effects – 75.70.-i Magnetic properties of thin films, surfaces, and interfaces – 75.50.Bb Fe and its alloys – 75.50.Ss Magnetic recording materials

1 Introduction

Studies of the magneto-optical Kerr effect (MOKE) are motivated either by the sensitivity of the Kerr effect to detect surface magnetism or by the potential use of this effect for high density recording system. Many studies are focused on the polar Kerr effect for vertical magneto-optic recording [1,2]. However, the longitudinal Kerr effect is also interesting for reading out magnetically stored information [3,4] or even as magnetic field sensor [5]. In both cases, high Kerr rotation and reflectivity are required. The enhancement of the rotation can be realized with magnetic films multilayered with dielectric spacers like SiO, SiO_2, Si_3N_4, Al_2O_3 when some conditions to make constructive interferences are satisfied [6–11]. Furthermore, it was shown that the metal/dielectric systems present some advantages over the metal/metal systems [12].

In this paper, we present experimental results on longitudinal MOKE, for s- and p-polarized incident light. The magneto-optical measurements of the multilayers used experimentally are predicted by using macroscopic approach calculations, based on a matrix formalism [13,14]. Optical and magneto-optical constants of each film have been determined, and large Kerr rotations are obtained with basic stacking design. The reflectivity and a figure of merit that combines Kerr rotation and reflectivity are also plotted against the Al_2O_3 thickness.

[a] e-mail: abourzami@yahoo.fr

2 Experimental procedures

$[Al_2O_3/Fe]_m$-films ($m = 1, 2$) were rf magnetron sputtered onto microelectronics-grade silicon Si(100), using an automated Alcatel SCM650 apparatus. The base pressure was 5×10^{-7} mbar. Then 99.999% purified argon is introduced into the chamber through a pressure-regulated valve. Fe and Al_2O_3 were sputtered from pure Fe and Al_2O_3 targets with respective applied rf powers of 200 W and 250 W. To achieve a good uniformity of deposition, the substrates were scanned 10 cm above the cathodes. The deposition rates of each material were measured *via* SAXS (small angle X-ray scattering) experiments [15]. In a first set of samples, Fe was deposited with various argon pressures. In a second series of samples, the Al_2O_3 thicknesses were varied while all other deposition conditions were kept constant ($P_{Ar} = 3 \times 10^{-3}$ mbar). An X-ray diffraction study showed that the Al_2O_3 was amorphous and the Fe was polycrystalline in the bcc phase [16].

Kerr rotation and ellipticity are measured *ex-situ* using the retardation modulation technique [17]. A He-Ne laser ($\lambda = 632.8$ nm) beam passes across a polarizer P, through a hole in the first electromagnet pole and illuminates the sample (maintained in vertical position) close to 69° to the normal. This incidence is chosen because initially the set-up is built for ellipsometric applications. The reflected beam passes through a hole in the second electromagnet pole and crosses successively a quarter-wave plate L, a photo-elastic modulator PEM [18] and an

analyzer A turned at 45° from P and from the s- and p-directions *i.e.*, the PEM-axes. The outgoing beam is detected with a photomultiplier PM having large sensitive area. The set-up described in reference [17] could calibrate only the rotation. We have then inserted a quarter-wave plate L to calibrate both Kerr rotation and ellipticity. The signal coming from the PM is analyzed with a lock-in amplifier, tuned on the PEM modulation frequency f.

Assuming the laser wave to be a monochromatic plane wave, and following the same method adopted by Sato [17], the electric field components for the transmitted wave, by the PEM, A and L elements, have been derived. Using the small angle approximation ($\tan\theta_{\rm K} \approx \theta_{\rm K}$ and $\sin\varepsilon_{\rm K} \approx \varepsilon_{\rm K}$) one will find that the detected intensity can be written as:

$$I(\Omega) = I_0[1 + 2(\gamma - \varepsilon_{\rm a} - \varepsilon_{\rm K}) \cdot \cos\varphi(t) + 2(\gamma + \theta_{\rm a} + \theta_{\rm K}) \cdot \sin\varphi(t)] \quad (1)$$

where: γ denotes the angle between L-axes and the s- and p-directions, $\theta_{\rm K}$ and $\varepsilon_{\rm K}$ are the Kerr rotation and ellipticity respectively, $\theta_{\rm a}$ and $\varepsilon_{\rm a}$ are respectively the rotation and ellipticity of the metallic layer and $\varphi(t) = \varphi_m \sin\Omega t$ represents the retardation introduced by the modulator with $\Omega = 2\pi f$. Note that the small angle approximation is valid, in our case, up to 10° angle which corresponds to a rotation $\theta_{\rm K}$ (or an ellipticity $\varepsilon_{\rm K}$) equal to 20° for an inversion of the applied magnetic field.

The development of $I(\Omega)$ up to the second harmonic in Ω gives:

$$I(\Omega) = I_0[1 + 2(\gamma - \varepsilon_{\rm a} - \varepsilon_{\rm K})J_0(\varphi_m)] + I_0[4(\gamma + \theta_{\rm a} + \theta_{\rm K})J_1(\varphi_m)]\sin\Omega t + I_0[4(\gamma - \varepsilon_{\rm a} - \varepsilon_{\rm K})J_2(\varphi_m)]\cos 2\Omega t.$$

$J_p(\varphi_m)$ are the Bessel functions of order p. By adjusting modulation level $\varphi_m = 2.405$ (so that $J_0(\varphi_m) = 0$), the signals issued from the lock-in amplifier (mode f and $2f$), normalized to the continuous component, are:

$$S_F(\gamma) = 4J_1(\varphi_m) \cdot (\gamma + \theta_{\rm a} + \theta_{\rm K}) \approx 2.08 \cdot (\gamma + \theta_{\rm a} + \theta_{\rm K})$$
$$S_{2F}(\gamma) = 4J_2(\varphi_m) \cdot (\gamma + \varepsilon_{\rm a} + \varepsilon_{\rm K}) \approx 1.72 \cdot (\gamma - \varepsilon_{\rm a} - \varepsilon_{\rm K}). \quad (2)$$

We show then that Kerr rotation $\theta_{\rm K}$ and the ellipticity $\varepsilon_{\rm K}$ are detected in mode "f" and mode "$2f$" respectively when we rotate the quarter-wave plate (unlike the case where the PEM rotates in Ref. [17]). The quarter wave plate is rotated with a stepping motor with 1 mdeg increment. $\theta_{\rm K}$ and $\varepsilon_{\rm K}$ are measured for an inversion of the applied magnetic field.

3 Experimental measurements

3.1 Refractive indices

We have measured the reflection spectrum between 550–800 nm of a thick Al_2O_3 film deposited onto a Si(100) using a Perkin-Elmer spectrophotometer. The obtained spectrum is then fitted by using the silicon optical constants [19] while the Al_2O_3 refractive index n_A is taken to vary as a function of the wavelength λ according to Cauchy formula:

$$n_A = A + \frac{B}{\lambda^2(\text{nm})} \cdot \quad (3)$$

The best fit of the spectrum is obtained for:

$$A = 1.62 \quad \text{and} \quad B = 0.014 \times 10^6\,(\text{nm})^2.$$

The evolutions with the argon pressure of the Fe optical constants (n_0, k) are determined by Kramers-Kronig analysis of reflectance at normal incidence on reflective Fe films. Reflection spectra are recorded in the full range (200–2600 nm) of a Perkin-Elmer spectrophotometer. Each film has a thickness greater than the skin depth.

In the Kramers-Kronig formalism [19] the integral:

$$\Phi = 2\frac{\lambda_0}{\pi}\int_0^\infty \frac{\ln R(\lambda) - \ln R(\lambda_0)}{\lambda^2 - \lambda_0^2}\,\mathrm{d}\lambda \quad (4)$$

which gives the phase Φ of the Fresnel reflection factor $r = \sqrt{R_0}\,\mathrm{e}^{i\Phi}$ for $\lambda = 632.8$ nm, is split into three regions:

(i) For high wavelengths ($\lambda > 2600$ nm): the reflection coefficient R is constant because, in this case, the conductor is well described by Drude's law. The contribution of this part is not taken into account.

(ii) The region that corresponds to experimental spectrum: the integral was evaluated numerically by the trapezoidal method.

(iii) For short wavelengths ($\lambda < 200$ nm): the integral was calculated by extrapolation of the reflection coefficient:

$$R(\lambda) = R(200) \cdot \left(\frac{\lambda(\text{nm})}{200}\right)^2. \quad (5)$$

Knowing the phase angle Φ and reflectivity R_0 at $\lambda = 632.8$ nm, the real and imaginary parts of refractive index, n_0 and k respectively, can be determined by solving the equation:

$$r = \sqrt{R_0}\,\mathrm{e}^{\mathrm{i}\Phi} = \frac{\tilde{n}_0 - 1}{\tilde{n}_0 + 1} = \frac{n_0 - 1 - \mathrm{i}k}{n_0 + 1 - \mathrm{i}k}$$

where $\tilde{n}_0 = n_0 - \mathrm{i}k$, we find:

$$n_0 = \frac{1 - R_0}{1 + R_0 - 2\sqrt{R_0}\cos\Phi}$$
$$\text{and} \quad k = -2\frac{\sqrt{R_0}\sin\Phi}{1 + R_0 - 2\sqrt{R_0}\cos\Phi} \cdot \quad (6)$$

3.2 Magneto-optical parameter

The complex magneto-optic parameter $Q = Q_1 - \mathrm{i}Q_2$ can be calculated from the next equation (Eq. (7)) giving the complex Kerr rotation $\tilde{\theta}_{\mathrm{K}s}$ for s-polarized incident light.

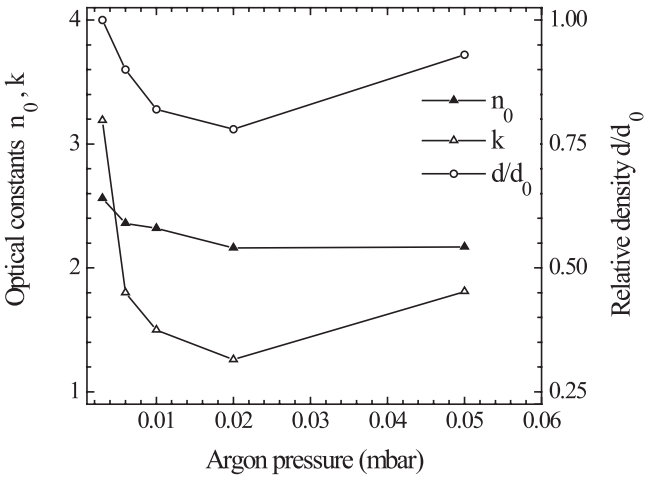

Fig. 1. Fe optical constants and relative density *vs.* argon pressure.

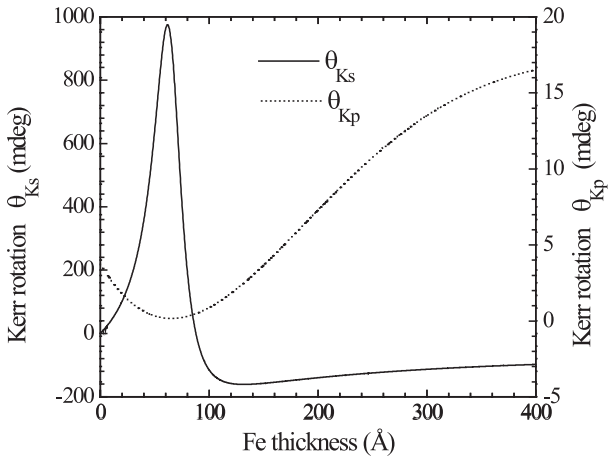

Fig. 2. Kerr rotations as a function of the Fe layer thickness t for Al_2O_3(1100 Å)/Fe(t)/Si sample.

In the case of the longitudinal MOKE configuration, $\tilde{\theta}_{\mathrm{K}s}$ is given to first order in Q by [20]:

$$\tilde{\theta}_{\mathrm{K}s} = \frac{\mathrm{i}\tilde{n}_0 w_y \cos\theta}{w_z(\tilde{n}_0\cos\theta + w_z)(\cos\theta - \tilde{n}_0 w_z)} Q \qquad (7)$$

where (w_y, w_z) are the direction cosines of the average direction of the refracted wave in the magnetic medium (Fe); w_y is related to the incidence angle θ by the Snell's refraction law: $w_y = \sin\theta/\tilde{n}_0$.

The measured Kerr rotation and ellipticity for a saturated sample deposited at 3×10^{-3} mbar argon pressure, are found to be equal to:

$$\theta_{\mathrm{K}s} = 154\,\mathrm{mdeg} \qquad \text{and} \qquad \varepsilon_{\mathrm{K}s} = 8\ \mathrm{mdeg}.$$

The obtained magneto-optic parameter is: $Q = 0.0355 - \mathrm{i}\,0.0016$.

The deduced values for $\tilde{n}_0 = n_0 - \mathrm{i}k$ and $Q = Q_1 - \mathrm{i}Q_2$ are close to those used in references [13] and [20].

4 Results and discussions

It is known that preparation conditions play an important role on the microstructure and on the magnetism of the Fe layers [21]. We therefore decided to determine the influence of the argon pressure during the process on the optical constant n_0 and k of Fe. In Figure 1, the optical constants (real and imaginary parts of the refractive index) and relative density d/d_0 (d and d_0 denote the density of the Fe film and bulk respectively) are plotted as a function of Ar pressure; d is deduced from SAXS experiment [15]. One can notice that the variations of the two optical constants follow the evolution of the relative density d/d_0 of the sample.

Once the effect of argon pressure is determined, Fe thin films with given optical constants can thus be prepared. In fact, the argon pressure during the process also affects the roughness of the layer. In the other experiments (the thickness effect), we have chosen $P_{\mathrm{Ar}} = 3 \times 10^{-3}$ mbar which leads to compact films (optical constants close to the bulk ones) and the lowest roughness. It is very difficult to deposit films below this argon pressure because of the plasma instabilities. Having chosen preparation conditions and determined optical and magneto-optical constants, we performed calculations to find out the optimum film thicknesses for enhancing the Kerr effect.

Kerr rotations ($\theta_{\mathrm{K}s}$ and $\theta_{\mathrm{K}p}$) are computed for the s- and p-polarizations using a macroscopic approach based on the knowledge of two matrices [13,14]. These simulations were performed for an incidence angle $\theta = 69°$ fixed on the experimental set-up.

The first step in the simulation consists in the determination of the optimal Fe layer thickness coated with a 1100 Å thick Al_2O_3.

This last thickness is chosen so as there will be an agreement between the phases of the two waves reflected respectively by the upper interface and the Al_2O_3/Fe one (*i.e.*, a constructive interference between the resulting waves reflected by each interface).

In Figure 2, theoretical results are presented, *i.e.*, the computed Kerr rotation is plotted against the Fe thickness t. In the s-polarization case, at small t, $\theta_{\mathrm{K}s}$-curve shows a linear behavior due to the Faraday effect. At large t, greater than the skin depth, the Faraday contribution breaks down and $\theta_{\mathrm{K}s}$ is fully determined by the Kerr effect in bulk. In the intermediate region, both these effects take place together and $\theta_{\mathrm{K}s}$ shows a peak for t close to 70 Å, due to interferences of the waves reflected by the upper interface and the substrate and the low value of the Fresnel factor r_{ss}, the ratio of the amplitude of s-polarized reflective wave to the incident one. The second extremum is lower than the first one because of our choice of alumina thickness. It corresponds to the interferences of the first wave and the one reflected by Al_2O_3/Fe interface. On the contrary, in the p-polarization case, very small oscillations are observed for $\theta_{\mathrm{K}p}$, which remains low because the incidence angle is close to the Brewster's angle.

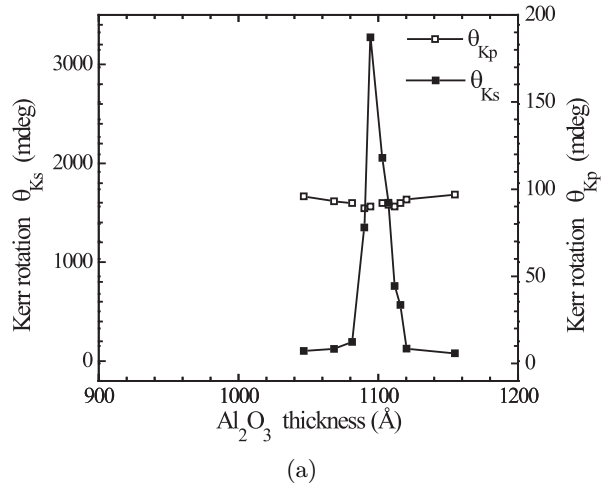

(a)

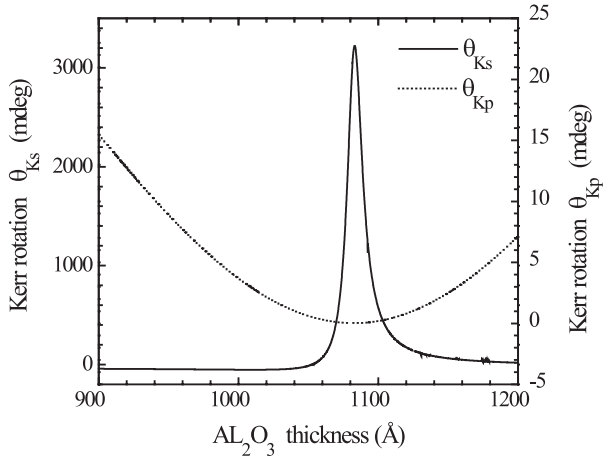

(b)

Fig. 3. Kerr rotations as a function of the Al_2O_3 layer thickness t_A for: (a) $Al_2O_3(t_A)$/Fe(51 Å)/Si sample (experimental curve). (b) $Al_2O_3(t_A)$/Fe(72 Å)/Si multilayer (theoretical curve).

Experimentally, to get a phase agreement between reflected waves, it is preferable to adjust the thickness of Al_2O_3 which is transparent, while keeping the magnetic layer thickness constant.

Calculations have then been performed in the aim to optimize the Al_2O_3 thickness t_A. The calculated Kerr rotations θ_{Ks} and θ_{Kp} *vs.* t_A in the case of $Al_2O_3(t_A)$/Fe(51 Å)/Si bilayers show that θ_{Kp} is practically insensitive to the Al_2O_3 thickness for the reason mentioned above (Brewster's angle). On the contrary, the curve $\theta_{Ks}(t_A)$ has a peak equal to 0.7°.

The experimental confirmation (Fig. 3a), for samples prepared by rf sputtering shows that θ_{Kp} remains quite low while θ_{Ks} has a maximum (3.2°) for t_A close to 1094 Å!

In Figure 3b we show calculated Kerr rotations θ_{Kp} and θ_{Ks} *vs.* t_A in the case of the $Al_2O_3(t_A)$ Fe(72 Å) /Si bilayer. The curve present a good fit for the experimental values.

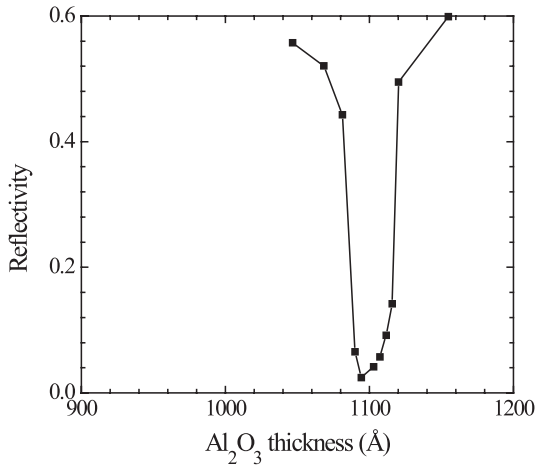

Fig. 4. Reflectivity as a function of the Al_2O_3 layer thickness t_A for: $Al_2O_3(t_A)$/Fe(51 Å)/Si sample.

Although large Kerr rotations are highly desirable, sufficient reflectivity is also required for Kerr measurements. The reflectivity is then plotted against the Al_2O_3 thickness (Fig. 4). The reflectivity is low because the Al_2O_3 thickness represents an anti-reflect (AR) layer.

In order to get large Kerr rotation and enhance reflectivity, we have to change the geometry of the sample and prepare iron/alumina multilayer:

$$Al_2O_3(t_{A2})/[Fe(t)/Al_2O_3(t_{A1})]/Fe(t)/Si.$$

The theoretical calculations give the thicknesses which correspond to the following sample:

$$Al_2O_3(t_A)/[Fe(37\,Å)/Al_2O_3(147\,Å)]/Fe(37\,Å)/Si.$$

We prepared it in the conditions mentioned in Section 2. Once more, the experimental values of θ_{Ks} are larger than the computed ones whereas the theoretical and experimental θ_{Kp} remain sensitively constant and low. Concerning θ_{Ks} (Fig. 5a), one can see experimentally a peak with the value 6.85° for an Al_2O_3 layer thickness t_A close to 973 Å.

The best fit of this curve is obtained by choosing the following Fe and Al_2O_3 thicknesses for the sample (Fig. 5b):

$$Al_2O_3(t_A)/[Fe(55\,Å)/Al_2O_3(134\,Å)]/Fe(46\,Å)/Si.$$

Moreover, the reflectivity curve for the quadrilayer is wide (Fig. 6). We can then choose a sample configuration which gives an important rotation with a sufficient reflectivity. Theoretically, the reflectivity can be enhanced by working in the vicinity of grazing incidence. Unfortunately, the angle of the incidence cannot be modified on our experimental set-up.

The figure of merit may be defined in many ways [2,8,12]. We have used the expression $F = R_{ss}\sin^2\theta_{Ks}$ which comprises both the *s*-polarized reflectivity R_{ss} and Kerr rotation θ_{Ks} to characterize the performance of the medium. In Figure 7, F is plotted against

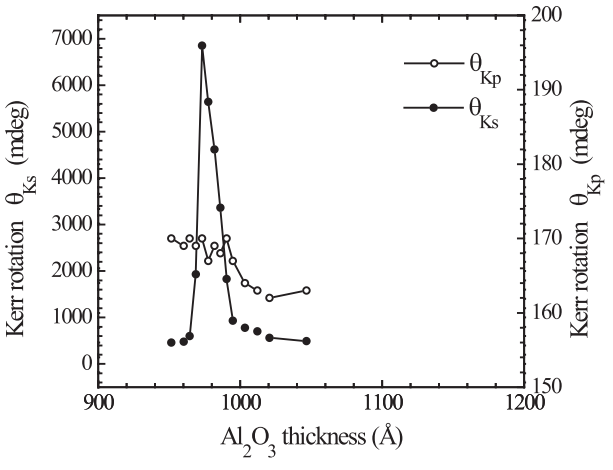

(a)

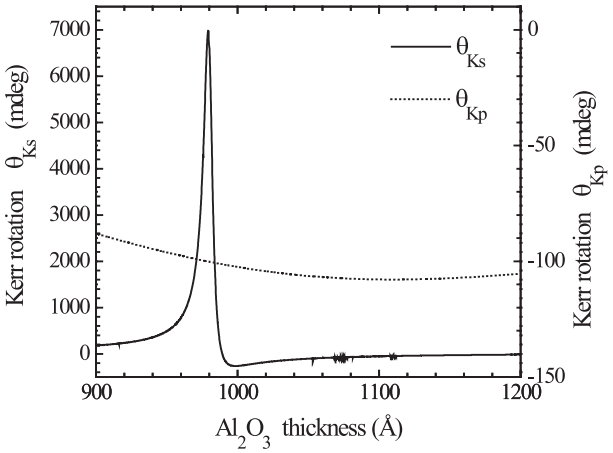

(b)

Fig. 5. Kerr rotations as a function of the Al_2O_3 layer thickness t_A for: (a) $Al_2O_3(t_A)$/ Fe(37 Å)/Al_2O_3 (147 Å)/Fe(37 Å)/Si sample (experimental curve). (b) $Al_2O_3(t_A)$/Fe(55 Å)/Al_2O_3 (134 Å)/Fe(46 Å)/ Si multilayer (theoretical curve).

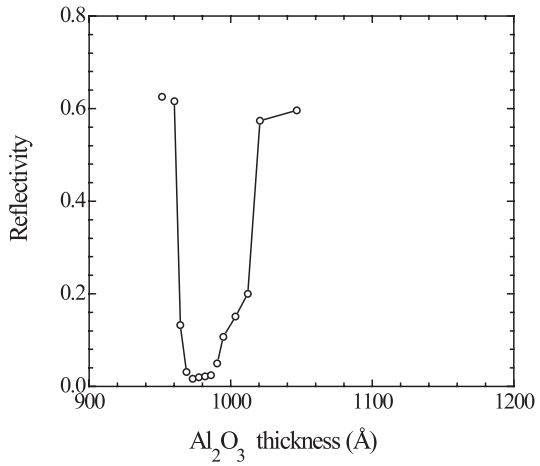

Fig. 6. Reflectivity as a function of the Al_2O_3 layer thickness t_A for $Al_2O_3(t_A)$/Fe(37 Å)/Al_2O_3(147 Å)/Fe(37 Å)/Si sample.

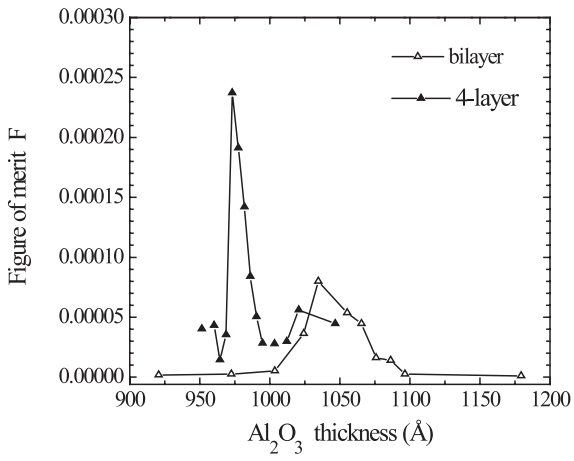

Fig. 7. Figure of merit, F, *vs.* Al_2O_3 thickness for: $Al_2O_3(t_A)$/Fe(51 Å)/Si bilayer (open triangle) and $Al_2O_3(t_A)$/Fe(37 Å)/Al_2O_3(147 Å)/Fe(37 Å)/Si quadrilayer (solid triangle).

the Al_2O_3 thickness for the two sets of samples. One can note that the figure of merit values are of the same order of magnitude as those reported in the literature (see, for example, Ref. [8]). Also, for the quadrilayer system, F shows a maximum which is three times the one corresponding to the bilayer system.

One can see for the two cases of multilayers that the experimental maximum θ_{Ks}-values are larger than the predicted ones, using thicknesses deduced from SAXS experiment. Moreover, for the bilayer Al_2O_3(1100 Å)]/Fe(75 Å)/Si prepared in mentioned conditions, we have observed a lower Kerr rotation θ_{Ks} than the predicted one.

The best fits are realized for large iron thicknesses. This effect is due to the fact that the magnetic iron thicknesses are larger than those deduced from SAXS experiment because of atomic diffusion of Fe atoms in Al_2O_3 and Si at the interfaces. Indeed, it was shown from Mössbauer spectroscopy in the case of $[Al_2O_3/Fe]_m$/Si multilayers that this magnetic iron thickness depends on Al_2O_3 film thickness and on the number m of bilayers [16].

Furthermore, the theoretical curves are slightly high and shifted with respect to the experimental ones. The difference in magnitude could be attributed to roughnesses. The roughness tends to reduce the magnitude of the Kerr rotation peak. In our simulations smooth interfaces are considered while in fact SAXS experiment shows the following roughnesses: $\sigma(\text{air}/Al_2O_3)$ = 12 Å, $\sigma(Al_2O_3/\text{Fe})$= 11 Å and $\sigma(\text{Fe/Si})$ = 6 Å.

Finally, the shifts ($\Delta t_A \approx 6$ Å) between the theoretical and experimental positions of the peaks result from

the uncertainty on the refractive index of alumina. This uncertainty is inevitable because it is related to alumina thickness error.

5 Conclusion

Our multilayered samples offer the possibility to modify optical and magneto-optical constants with the sputtering parameters. Simulations have been applied to $[Al_2O_3/Fe]_m/Si$ samples ($m = 1, 2$) as a function of the upper Al_2O_3 layer thickness in order to find out the best sample parameters which will give high Kerr rotations. The optical and magneto-optical constants of each layer are first determined experimentally. For an incidence angle close to the Brewster's angle, we show that Kerr rotation in only *s*-polarized light can be amplified by multireflections. One can deduce that for an incidence angle equal to the Brewster's angle, polarized incident light is not required for observing Kerr effect. There is a fairly better agreement between experimental results and theoretical fits using Fe magnetic thicknesses than those using thicknesses deduced from SAXS experiment; this difference in thicknesses is due to the atomic diffusion of Fe in Al_2O_3 and Si at interfaces.

A longitudinal Kerr rotation close to 7° is observed in $Al_2O_3/Fe/Al_2O_3/Fe/Si$ multilayer. An improvement of the figure of merit is observed for the quadrilayer compared to the bilayer one. Our theoretical and experimental methods are easily applied to any samples in order to get high Kerr rotation or ellipticity. The reflectivity can be enhanced by using good reflectors as substrates. Furthermore, grazing angles of incidence provide theoretically higher reflectivities but slightly lower Kerr rotations. A figure of merit analysis of this has not yet been done. Also, a complete study should take into account the effect of the roughness of all interfaces.

References

1. B.S. Kruor, G.A.N. Connel, *Transition metal Alloys for M.O. Recording* (Academic Press Inc., 1991), 143 p. (ISBN 0-12-533015-4)
2. E.R. Moog, J. Zak, S.D. Bader, J. Appl. Phys. **69**, 880 (1991)
3. F. LeTexier, C. Maillot, J. Appl. Phys. **73**, 6238 (1993)
4. J.P. Castera, *Couches minces et Multicouches Magnétiques*, Colloque Louis Néel (Thomson-CSF, 1974)
5. J. Pistora, private communication
6. R. Sato, N. Saito, T. Morishita, IEEE Trans. Magn. **24**, 2458 (1988)
7. M. Nyvlt, J. Ferré, J.P. Jamet, P. Houdy, P. Boher, S. Visnovsky, R. Urban, R. Lopusnik, J. Magn. Magn. Mater. **156**, 175 (1996)
8. C. Gueugnon, P. Bernstein, R. Lefèbre, J. Appl. Phys. **57**, 3891 (1985)
9. R. Krishnan, J. Magn. Magn. Mater. **109**, 64 (1992)
10. G.A.N. Connel, Appl. Phys. Lett. **40**, 212 (1982)
11. K. Otha, *et al.*, Proc. SPIE **382**, 252 (1983)
12. R. Atkinson, J. Magn. Magn. Mater. **124**, 333 (1993)
13. J. Zak, E.R. Moog, C. Liu, S.D. Bader, J. Magn. Magn. Mater. **89**, 107 (1990)
14. A. Bourzami, O. Lenoble, Ch. Fery, J.F. Bobo, M. Piecuch, Phys. Rev. B **59**, 11489 (1999)
15. M. Piecuch, L. Nevot, Mater. Sci. Forum **59-60**, 93 (1990)
16. O. Lenoble, J.F. Bobo, L. Hennet, H. Fischer, Ph. Bauer, M. Piecuch, Thin Solid films **275**, 64 (1996)
17. K. Sato, Jap. J. Appl. Phys. **20**, 2403 (1981)
18. J. Badoz, M. Billardon, J.C. Canit, M.F. Russel, J. Opt. **8**, 373 (1977)
19. E.D. Palik, *Handbook of Optical Constants of Solids* (Academic Press Inc., London 1985), pp. 56, 229 and 565
20. G. Metzger, P. Pluvinage, R. Torquet, Ann. Phys. **10**, 5 (1965)
21. Ch. Féry, L. Hennet, O. Lenoble, M. Piecuch, E. Snoeck, J.F. Bobo, J. Phys. C **10**, 6629 (1998)